An Improved Observer-Based Current Decoupling Method for Mitigating Speed Fluctuation of Variable Flux Memory Machines

Yuxiang Zhong, Heyun Lin, *Senior Member, IEEE*, Jiyao Wang, *Member, IEEE*, Wei Liu, Hui Yang, *Senior Member, IEEE*, and Xiping Liu

***Abstract*—Variable flux memory machines (VFMMs) usually need to inject *d*-axis current pulses in the stator windings to conduct magnetization state (MS) manipulations, which inevitably causes large torque pulsation and speed fluctuation especially under load condition. In this article, an improved observer-based current decoupling method is proposed to calculate the *q*-axis current (i_q) reference for speed fluctuation mitigation based on the estimated *dq*-axis flux linkages. Specifically, an improve stator current observer with a supertwisting sliding mode regulator is structured to more accurately estimate the voltage disturbances caused by parameter mismatches. Then, the *dq*-axis flux linkages are decoupled from the voltage disturbances estimated by the current observer, considering dynamic changes of PM flux linkage and inductances during MS manipulations. Based on the estimated *dq*-axis flux linkages, an i_q reference can be calculated according to the torque equation and the divergence of i_q can be avoided by using a piecewise function when the denominator is close to 0. Finally, the effectiveness and feasibility of the proposed method are validated through both simulation and experimental measurements on a separated series–parallel VFMM.**

***Index Terms*—Flux linkage observer, magnetization state (MS) manipulation, observer-based current decoupling, speed regulation, variable flux memory machine (VFMM).**

I. Introduction

WIDE speed operation is required for electrical machines in many applications, such as electrical vehicles and flywheel energy storage. For conventional permanent magnet synchronous machines (PMSMs) [1], [2], [3], [4], [5], [6], flux-weakening control [4], [5], [6] is commonly used to achieve high-speed operation by applying a continuous *d*-axis current to reduce the terminal voltage. However, it will unavoidably cause additional copper loss and thus reduce the efficiency at high-speed region. Therefore, various variable flux memory machines (VFMMs) are proposed in [7], [8], [9], [10], [11], [12], [13], [14], [15], [16], [17], [18], [19], [20], [21], [22] to achieve "true" wide speed operation. This type of machine has adjustable permanent magnet (PM) flux linkage, benefiting from the equipped low coercive force PMs, such as AlNiCo, of which the magnetization state (MS) can be flexibly changed by applying *d*-axis current pulses. Compared with conventional flux-weakening control used in PMSM, this approach to change the PM flux linkage does not require a continuous flux-weakening current at high-speed region and consequently improve the overall efficiency.

Commonly, VFMM is magnetized to a high MS at low-speed region to output the high torque, and is demagnetized to a low MS at high-speed region to reduce the copper loss and extend the speed range. This process of changing MS, also called MS manipulation, is considered as the critical step to guarantee that the machine operates at optimal MS. During MS manipulation, a *d*-axis current pulse, commonly three or four times of the rated current, is applied into the stator windings. Although it only lasts a few tens of milliseconds, unwanted large torque pulsation and speed fluctuation will be caused under load condition, degrading the dynamic performance of VFMM drive system.

In order to address the abovementioned problems, several MS manipulation methods have been proposed [10], [11], [12], [13]. In [10], [11], [12], MS manipulations are conducted under zero speed and zero load conditions or by using premeasured current vector trajectories under nonzero speed and load conditions. The former method is unpractical since it cannot work under load conditions. The latter method has to adopt a lot of lookup tables to store the current trajectories in the processor, which not only should be obtained in advance through time-intensive experiments, but also calibrated frequently against parameter variations. An observer-based current decoupling method is proposed in [13] to achieve smooth torque control during MS manipulations under load conditions. Specifically, the estimation of *dq*-axis flux linkages is achieved by using the voltage

Manuscript received 6 June 2023; revised 18 September 2023; accepted 11 November 2023. Date of publication 14 November 2023; date of current version 22 December 2023. This work was supported in part by the National Natural Science Foundation of China under Grants 52037002 and 52077033, in part by the Key R&D Program of Jiangsu Province under Grant BE2021052, in part by the "Thousand Talents Plan" Project of Jiangxi Province under Grant jxsq2020102088, and in part by the GF (Guofang) Key Laboratory of Science and Technology Foundation Project under Grant 6142217210201. Recommended for publication by Associate Editor S. A. Khajehoddin. *(Corresponding author: Heyun Lin.)*

Yuxiang Zhong, Heyun Lin, Jiyao Wang, and Hui Yang are with the School of Electrical Engineering and Suzhou Institute, Southeast University, Nanjing 210096, China (e-mail: zhongyx@seu.edu.cn; hyling@seu.edu.cn; jyaowang@seu.edu.cn; huiyang@seu.edu.cn).

Wei Liu is with the Ningbo Institute of Materials Technology and Engineering, Chinese Academy of Sciences, Ningbo 315000, China (e-mail: lwei@nimte.ac.cn).

Xiping Liu is with the School of Electrical Engineering and Automation, Jiangxi University of Science and Technology, Ganzhou 341000, China (e-mail: liuxiping@jxust.edu.cn).

Color versions of one or more figures in this article are available at https://doi.org/10.1109/TPEL.2023.3332728.

Digital Object Identifier 10.1109/TPEL.2023.3332728

disturbances estimated by stator current observers. Then, q-axis current reference can be decoupled according to the electromagnetic torque equation and estimated flux linkages. With the help of the flux linkage observer, this method is robust to machine parameter variations and does not require the cumbersome lookup tables. In [14], an active disturbance rejection speed controller combining model compensation is newly structured to mitigate the speed fluctuations during MS manipulations.

The observer-based method in [13] seems quite appropriate for VFMMs since their parameter variations are more prominent than those of conventional PMSMs. However, some challenging problems should be well addressed to achieve satisfactory control performance. First, it is difficult for the stator current observer to accurately estimate the injected d-axis current pulse under different operating conditions. Second, when estimating the dq-axis flux linkages from the voltage disturbances, the dynamic changes of inductances and PM flux linkage during MS manipulations are neglected, which will cause large estimation errors. Third, when using the electromagnetic torque equation to calculate the q-axis current reference directly by division, the denominator might be 0 during MS manipulation, causing divergence of q-axis current and large speed fluctuation consequently. Therefore, an improved observer-based current decoupling method is proposed in this article to further reduce the speed fluctuations caused by MS manipulations. First, a supertwisting sliding mode (STSM) regulator is utilized to replace the proportional–integral (PI) regulator in conventional current observer, so that the current estimation accuracy can be significantly improved. Then, the dynamic changes of machine parameters during MS manipulations are considered to reduce the estimation errors when estimating the dq-axis stator flux linkages. Third, a novel current decoupling method is proposed to completely decouple the q-axis current reference based on the defined active flux linkage [24], and the divergence of q-axis current is avoided by adopting piecewise function.

The rest of this article is organized as follows. In Section II, the properties of the investigated separated series–parallel VFMM (SSP-VFMM) [9] are intuitively illustrated, including the topology and MS manipulation characteristics. In Section III, the conventional observer-based current decoupling method [13] is analyzed in detail and its shortcomings are summarized. In Section IV, the proposed method is demonstrated and interpreted with the help of diagrams and formulas. In Sections V and VI, simulation and experimental results on the SSP-VFMM prototype will be used to validate the effectiveness and feasibility of the proposed method.

II. SPP-VFMM Properties

A. Machine Topology

The topology of the investigated SSP-VFMM [9] with dual-layer PMs is shown in Fig. 1. The designed dual PM layers can obtain both the satisfactory field adjustment range and the excellent accidental demagnetization withstand capability. More details can be found in [9].

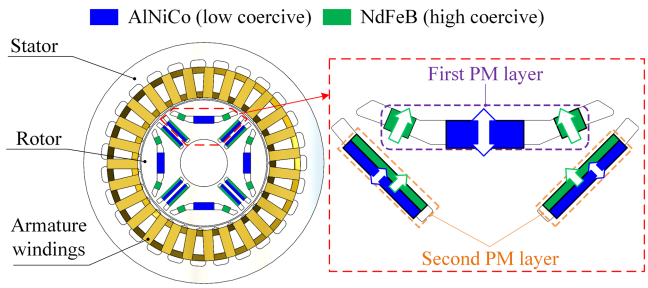

Fig. 1. Topology of investigated SSP-VFMM [9].

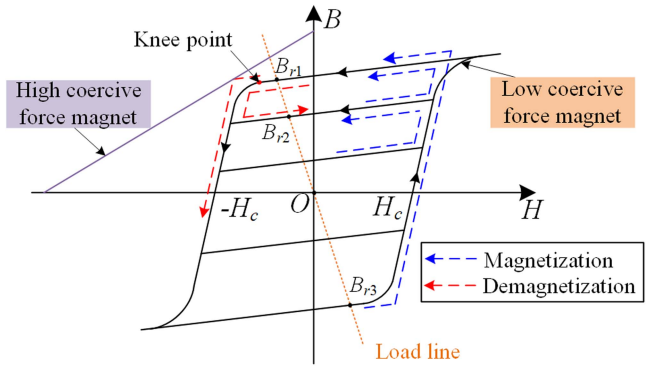

Fig. 2. Simplified hysteresis model of low coercive force magnets.

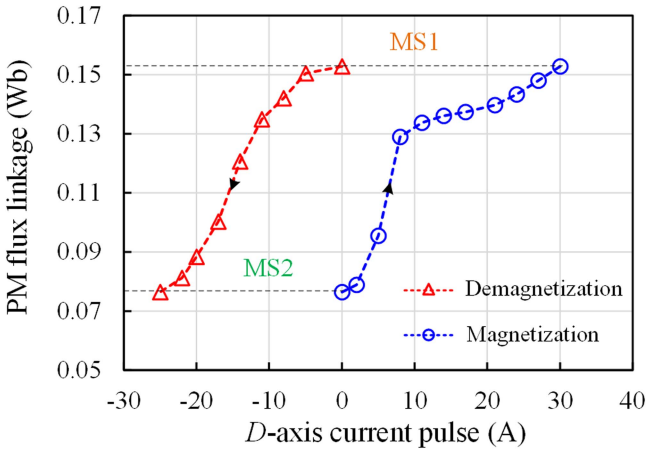

Fig. 3. Relation between the PM flux linkage and d-axis current pulse of the SSP-VFMM [9].

B. MS Manipulation Characteristics

A simplified hysteresis model of low coercive force magnets is shown in Fig. 2 to illustrate the flux regulation principle of VFMM. More details can be found in [20].

Fig. 3 shows the relation between the PM flux linkage and d-axis current pulse of the studied SSP-VFMM. Only two specific MSs, i.e., MS1 (0.153 Wb) and MS2 (0.076 Wb), are chosen to avoid frequent MS manipulations and thus reduce energy losses. The machine can be magnetized from MS2 to MS1 by applying a +30 A d-axis current pulse, and be demagnetized from MS1 to MS2 by applying a –25 A d-axis current pulse. The

required current pulses will cause a little increase in the cost of the inverter, which is totally acceptable since the speed range is significantly extended. Although these current pulses are several times of the rated current, they will not cause the noticeable temperature rise and damage the inverter due to the short time duration (only tens of milliseconds). Besides, the researchers are also focusing on the machine topology design of VFMM with the goal of further reducing the amplitude of the required current pulses.

III. Analysis of Conventional Stator Flux Linkage Observer and Q-Axis Current Decoupling Method

A. Mathematical Model of VFMM

The voltage equation of VFMM in the *d*-*q* reference frame can be expressed as

$$\begin{cases} u_d = Ri_d + \frac{d\psi_d}{dt} - \omega_e \psi_q \\ u_q = Ri_q + \frac{d\psi_q}{dt} + \omega_e \psi_d \end{cases} \tag{1}$$

where u_d and u_q are the *dq*-axis voltages, i_d and i_q are the *dq*-axis currents, R is the phase resistance, ω_e is the rotor electrical angular speed, ψ_d and ψ_q are the *dq*-axis stator flux linkages, which are expressed as

$$\begin{cases} \psi_d = L_d i_d + \psi_{\mathrm{PM}}(i_{d\_\mathrm{pulse}}) \\ \psi_q = L_q i_q \end{cases} \tag{2}$$

where L_d and L_q are the real *dq*-axis inductances, and $\psi_{\mathrm{PM}}(i_{d\_\mathrm{pulse}})$ is the variable PM flux linkage determined by the amplitude of i_d pulse, i_{d_pulse}.

The electromagnetic torque T_e and mechanical motion equation of the VFMM can be respectively expressed as

$$T_e = \frac{3}{2} p(\psi_d i_q - \psi_q i_d) \tag{3}$$

$$T_e - T_L - B\omega_m = J\frac{d\omega_m}{dt} \tag{4}$$

where p is the number of pole pairs, T_L is the load torque, B is the viscous friction coefficient, ω_m is the rotor mechanical angular speed, and J is the moment of inertia.

B. Conventional Stator Flux Linkage Observer

The voltage disturbance decoupling (VDD)-based stator flux linkage observer in [13] consists of three components, i.e., stator current observer, VDD and cascaded stator flux linkage observer. The details about the three parts are shown as follows.

Substituting (1) to (2) with the nominal constant values of the variables and neglecting the derivative terms [13], we have

$$\begin{cases} u_d = R_N i_d - \omega_e L_{qN} i_q + \Delta u_{d\_\mathrm{dis}} \\ u_q = R_N i_q + \omega_e L_{dN} i_d + \omega_e \psi_{\mathrm{PMN}} + \Delta u_{q\_\mathrm{dis}} \end{cases} \tag{5}$$

where the subscript "*N*" denotes the nominal constant value of the variable, $\Delta u_{d\_\mathrm{dis}}$ and $\Delta u_{q\_\mathrm{dis}}$ are the *dq*-axis voltage disturbances caused by parameter mismatches. If the resistance does not vary much, the *dq*-axis voltage disturbances can be expressed as

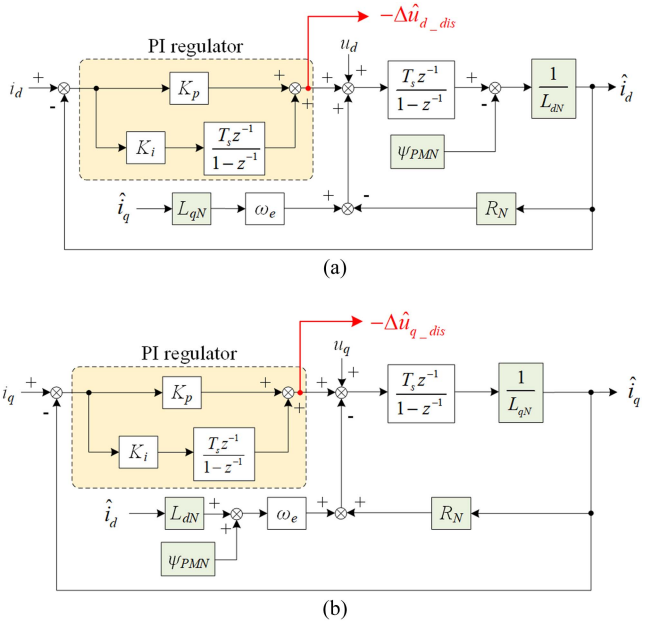

Fig. 4. Structure of conventional stator current observer with PI regulator. (a) *D*-axis observer. (b) *Q*-axis observer.

$$\begin{cases} \Delta u_{d\_\mathrm{dis}} = -\omega_e \Delta L_q i_q = -\omega_e \Delta\psi_q \\ \Delta u_{q\_\mathrm{dis}} = \omega_e(\Delta L_d i_d + \Delta\psi_{\mathrm{PM}}) = \omega_e \Delta\psi_d \end{cases} \tag{6}$$

where $\Delta L_d = L_d$–L_{dN}, $\Delta L_q = L_q$–L_{qN}, and $\Delta\psi_{\mathrm{PM}} = \psi_{\mathrm{PM}}(i_{d\_\mathrm{pulse}})$–$\psi_{\mathrm{PMN}}$ are the parameter variations, $\Delta\psi_d$ and $\Delta\psi_q$ are the differences between the real and nominal *dq*-axis stator flux linkages, respectively. To avoid the influences of resistance variation, a temperature-based resistance model or the stator resistance adaption method in [27] can be integrated into the proposed method to compensate for it.

A Luenberger-style current observer, as shown in Fig. 4, is constructed to estimate the *dq*-axis currents accurately based on (5), so that $\Delta u_{d\_\mathrm{dis}}$ and $\Delta u_{q\_\mathrm{dis}}$ can also be estimated simultaneously, which can be expressed as

$$\begin{cases} \Delta\hat{u}_{d\_\mathrm{dis}} = -\omega_e \Delta\hat{L}_q \hat{i}_q = -\omega_e \Delta\hat{\psi}_q \\ \Delta\hat{u}_{q\_\mathrm{dis}} = \omega_e(\Delta\hat{L}_d \hat{i}_d + \Delta\hat{\psi}_{\mathrm{PM}}) = \omega_e \Delta\hat{\psi}_d \end{cases} \tag{7}$$

where the superscript "^" denotes the estimated values of variables, $\Delta\hat{u}_{d\_\mathrm{dis}}$ and $\Delta\hat{u}_{q\_\mathrm{dis}}$ are the outputs of the PI regulators, $\Delta\hat{L}_d = \hat{L}_d - L_{dN}$, $\Delta\hat{L}_q = \hat{L}_q - L_{qN}$, $\Delta\hat{\psi}_{\mathrm{PM}} = \hat{\psi}_{\mathrm{PM}} - \psi_{\mathrm{PMN}}$, $\Delta\hat{\psi}_d$ and $\Delta\hat{\psi}_q$ are the differences between the estimated and nominal values of *dq*-axis stator flux linkages, respectively.

Assuming the estimated currents can track the real values accurately, it can be attained that

$$\begin{cases} \Delta\hat{\psi}_d = \Delta\psi_d \\ \Delta\hat{\psi}_q = \Delta\psi_q. \end{cases} \tag{8}$$

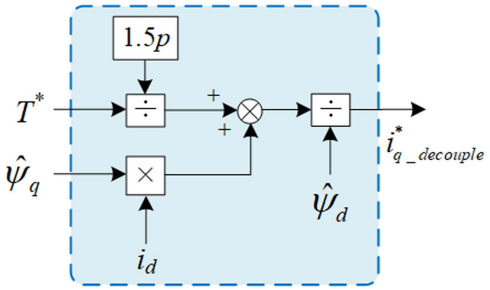

Fig. 5. Structure of conventional current decoupling method [13].

According to (7), $\Delta\hat{\psi}_d$ and $\Delta\hat{\psi}_q$ can be easily decoupled from the estimated voltage disturbances, as

$$\begin{cases} \Delta\hat{\psi}_d = \frac{\Delta\hat{u}_{q\_\text{dis}}}{\omega_e} \\ \Delta\hat{\psi}_q = -\frac{\Delta\hat{u}_{d\_\text{dis}}}{\omega_e}. \end{cases} \tag{9}$$

After obtaining $\Delta\hat{\psi}_d$ and $\Delta\hat{\psi}_q$, a Gopinath-style flux linkage observer based on voltage model, is cascaded with the stator current observer to reduce the parameter sensitivity during transient conditions and attain a better estimation performance [23].

C. Conventional Current Decoupling Method

The structure of the current decoupling method [13] is shown in Fig. 5. The q-axis current is decoupled based on (3) and can be calculated as

$$i^*_{q\_\text{decouple}} = \frac{T^*/(1.5p) + \hat{\psi}_q i_d}{\hat{\psi}_d} \tag{10}$$

where T^* is the reference torque, which is the output of the speed controller.

D. Analysis of Conventional Method

For the conventional flux observer and current decoupling method, there are three aspects requiring improvements for better control performance due to the unique MS manipulations of VFMM, which can be summarized as follows.

1) It is challenging for the stator current observer with PI regulator to estimate the currents accurately when injecting large i_d pulses under different conditions, thereby causing relatively large estimation errors of voltage disturbances.
2) When estimating $\Delta\psi_d$ and $\Delta\psi_q$ with the conventional VDD method during MS manipulations, the derivative terms, including the dynamic variations of inductances and PM flux linkage, are neglected, which will cause large estimation errors of flux linkages and thus degrade the speed fluctuation mitigation performance.
3) When using the conventional current decoupling method in (10), the divergence problem will be caused since the denominator $\hat{\psi}_d$ might be 0 during the demagnetization process, which is a unique problem for VFMM. Besides, i_q is not completely decoupled since i_q is involved in ψ_q in (10).

To address the abovementioned problems, an improved observer-based decoupling method is proposed considering the unique MS manipulations of VFMM to further mitigate the speed fluctuations.

IV. Proposed Stator Flux Linkage Observer and Current Decoupling Method

A. Stator Current Observer Considering Dynamic Parameter Variations

Substituting (2) to (1), the dq-axis voltage equation considering the dynamic variations of machine parameters can be expressed as

$$\begin{cases} u_d = \underbrace{Ri_d - \omega_e L_q i_q}_{\text{steadypart}} + \underbrace{L_d\frac{di_d}{dt} + i_d\frac{dL_d}{dt} + \frac{d\psi_{\text{PM}}(i_{d\_\text{pulse}})}{dt}}_{\text{dynamicpart}} \\ u_q = \underbrace{Ri_q + \omega_e[L_d i_d + \psi_{\text{PM}}(i_{d\_\text{pulse}})]}_{\text{steadypart}} + \underbrace{L_q\frac{di_q}{dt} + i_q\frac{dL_q}{dt}}_{\text{dynamicpart}}. \end{cases} \tag{11}$$

Both of the dq-axis voltages include two parts, i.e., steady and dynamic (derivative terms) ones. In traditional PMSMs, the dynamic parts are relatively small so that they are commonly neglected [23]. However, in VFMMs, the PM flux linkage and machine inductances will change drastically when MS manipulations are conducted with the injections of large i_d pulses. Therefore, the dynamic parts should be taken into account.

Using the nominal constant values of variables and considering the dynamic parts, (11) can be rewritten as

$$\begin{cases} u_d = R_N i_d + L_{dN}\frac{di_d}{dt} - \omega_e L_{qN} i_q + \Delta u_{d\_\text{dis}} \\ u_q = R_N i_q + L_{qN}\frac{di_q}{dt} + \omega_e(L_{dN} i_d + \psi_{\text{PMN}}) + \Delta u_{q\_\text{dis}}. \end{cases} \tag{12}$$

Then, Δu_{d_dis} and Δu_{q_dis} can be formed as

$$\begin{cases} \Delta u_{d\_\text{dis}} = \underbrace{\Delta L_d\frac{di_d}{dt} + i_d\frac{d\Delta L_d}{dt} + \frac{d\Delta\psi_{\text{PM}}}{dt}}_{\Delta u_{d\_\text{dis\_dyn}}} - \underbrace{\omega_e\Delta L_q i_q}_{\Delta u_{d\_\text{dis\_ste}}} \\ \quad = \frac{d\Delta\psi_d}{dt} - \omega_e\Delta\psi_q \\ \Delta u_{q\_\text{dis}} = \underbrace{\Delta L_q\frac{di_q}{dt} + i_q\frac{d\Delta L_q}{dt}}_{\Delta u_{q\_\text{dis\_dyn}}} + \underbrace{\omega_e(\Delta L_d i_d + \Delta\psi_{\text{PM}})}_{\Delta u_{q\_\text{dis\_ste}}} \\ \quad = \frac{d\Delta\psi_q}{dt} + \omega_e\Delta\psi_d \end{cases} \tag{13}$$

where $\Delta u_{d\_\text{dis\_dyn}}$ and $\Delta u_{d\_\text{dis\_ste}}$ are the dynamic and steady parts of Δu_{d_dis}, respectively, $\Delta u_{q\_\text{dis\_dyn}}$ and $\Delta u_{q\_\text{dis\_ste}}$ are the dynamic and steady parts of Δu_{q_dis}, respectively.

Similarly, the stator current observer is constructed as follows:

$$\begin{cases} u_d = R_N\hat{i}_d + L_{dN}\frac{d\hat{i}_d}{dt} - \omega_e L_{qN}\hat{i}_q + \Delta\hat{u}_{d\_\text{dis}} \\ u_q = R_N\hat{i}_q + L_{qN}\frac{d\hat{i}_q}{dt} + \omega_e(L_{dN}\hat{i}_d + \psi_{\text{PMN}}) + \Delta\hat{u}_{q\_\text{dis}}. \end{cases} \tag{14}$$

To improve the estimation accuracy, an STSM regulator [25], [26] is utilized to replace the conventional PI regulator, since it features good dynamic performance, low sliding mode chattering and is easily tuned. The structure of the stator current observer with the STSM regulator is shown in Fig. 6. With the

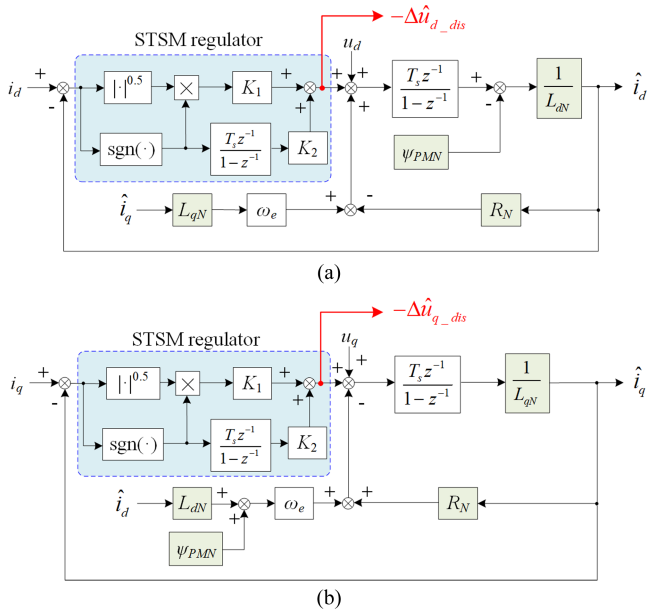

Fig. 6. Structure of proposed stator current observers with STSM regulators. (a) *D*-axis observer. (b) *Q*-axis observer.

help of the STSM regulator, the estimated currents can better track their real values during MS manipulations, so that $\Delta\hat{u}_{d\_\text{dis}}$ and $\Delta\hat{u}_{q\_\text{dis}}$ are closer to the real values. As the outputs of the STSM regulators, they can be expressed as

$$\begin{cases} \Delta\hat{u}_{d\_\text{dis}} = K_1|\tilde{i}_d|^{1/2}\text{sgn}(\tilde{i}_d) + K_2\int \text{sgn}(\tilde{i}_d)dt \\ \Delta\hat{u}_{q\_\text{dis}} = K_1|\tilde{i}_q|^{1/2}\text{sgn}(\tilde{i}_q) + K_2\int \text{sgn}(\tilde{i}_q)dt \end{cases} \tag{15}$$

where sgn(·) is the symbol function, $\tilde{i}_d = i_d - \hat{i}_d$ and $\tilde{i}_q = i_q - \hat{i}_q$ are the *dq*-axis current estimation errors, respectively, and K_1, and K_2 are the positive coefficients of the regulators, which are commonly designed as [25], [26]

$$K_1 = 1.5L^{1/2}, K_2 = 1.1L \tag{16}$$

where L is the boundary value of perturbation, and $L > 0$.

According to (13), it can be deduced that

$$\begin{cases} \Delta\hat{u}_{d\_\text{dis}} = \frac{d\Delta\hat{\psi}_d}{dt} - \omega_e\Delta\hat{\psi}_q \\ \Delta\hat{u}_{q\_\text{dis}} = \frac{d\Delta\hat{\psi}_q}{dt} + \omega_e\Delta\hat{\psi}_d. \end{cases} \tag{17}$$

When the estimated currents can track the real values accurately, (8) can be satisfied.

Then, the structure of the proposed VDD method based on (17) is illustrated in Fig. 7. Specifically, the discrete-time model of (17) using the backward difference method can be expressed as

$$\begin{cases} \frac{\Delta\hat{\psi}_d(k)-\Delta\hat{\psi}_d(k-1)}{T_s} - \omega_e\Delta\hat{\psi}_q(k) = \Delta\hat{u}_{d\_\text{dis}}(k) \\ \frac{\Delta\hat{\psi}_q(k)-\Delta\hat{\psi}_q(k-1)}{T_s} + \omega_e\Delta\hat{\psi}_d(k) = \Delta\hat{u}_{q\_\text{dis}}(k) \end{cases} \tag{18}$$

where k is the index of discrete sampling instant, and T_s is the sampling time.

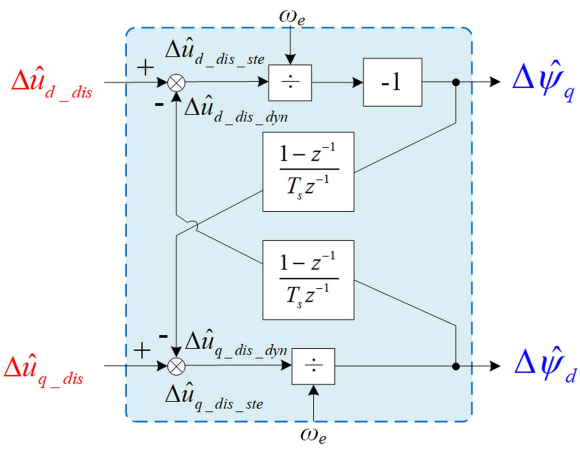

Fig. 7. Structure of proposed VDD method considering the dynamic changes of machine parameters.

Furthermore, $\Delta\hat{\psi}_d$ and $\Delta\hat{\psi}_q$ at time k can be calculated by

$$\begin{cases} \Delta\hat{\psi}_d(k) \\ = \frac{\Delta\hat{\psi}_d(k-1)+\Delta\hat{u}_{d\_\text{dis}}(k)T_s+\omega_e T_s\Delta\hat{\psi}_q(k-1)+\omega_e T_s^2\Delta\hat{u}_{q\_\text{dis}}(k)}{1+\omega_e^2T_s^2} \\ \Delta\hat{\psi}_q(k) \\ = \frac{\Delta\hat{\psi}_q(k-1)+\Delta\hat{u}_{q\_\text{dis}}(k)T_s-\omega_e T_s\Delta\hat{\psi}_d(k-1)-\omega_e T_s^2\Delta\hat{u}_{d\_\text{dis}}(k)}{1+\omega_e^2T_s^2}. \end{cases} \tag{19}$$

In the experiments, two low-pass filters with an appropriately designed cutoff frequency can be used to suppress the noise caused by the derivative terms.

B. New Observer-Based Current Decoupling Method During MS Manipulations

Substituting (2) into (3), we have

$$T_e = \frac{3}{2}pi_q\underbrace{[\psi_{\text{PM}}(i_{d\_\text{pulse}}) + (L_d - L_q)i_d]}_{\psi_{\text{act}}} \tag{20}$$

where ψ_{act} is the defined active flux linkage [24]. With the estimated *dq*-axis stator flux linkages, the active flux linkage can be then estimated as

$$\hat{\psi}_{\text{act}} = \hat{\psi}_{\text{PM}} + (\hat{L}_d - \hat{L}_q)i_d = \hat{\psi}_d - \hat{L}_q i_d. \tag{21}$$

In estimating$\hat{L}_q$, the amplitude of i_q should be considered to avoid the divergence of i_q. When the amplitude of i_q is relatively small (e.g., smaller than the preset threshold value, $i_{q\text{th}}$), the value of L_q is taken as L_{q0}, which can be measured under no load condition. Specifically, the estimated $\hat{L}_q$ can be expressed as

$$\hat{L}_q = \begin{cases} L_{q0}, & |i_q| < i_{q\text{th}} \\ \frac{\hat{\psi}_q}{i_q}, & |i_q| \geq i_{q\text{th}}. \end{cases} \tag{22}$$

Since $L_d < L_q$ in the studied SSP-VFMM, the value of ψ_{act} will change from positive to negative during the magnetization process of injecting a +30 A i_d pulse. This unique problem has been first reported in [20] by our research group and is defined as torque reverse phenomenon. In this case ($\psi_{\text{act}} < 0$), i_q

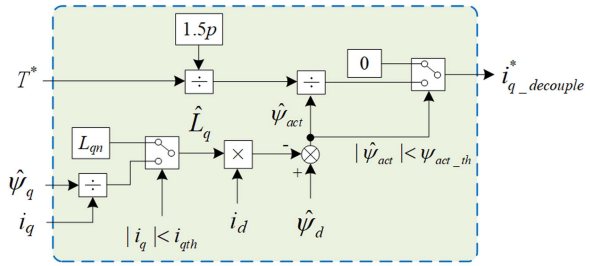

Fig. 8. Schematic diagram of the proposed current decoupling method.

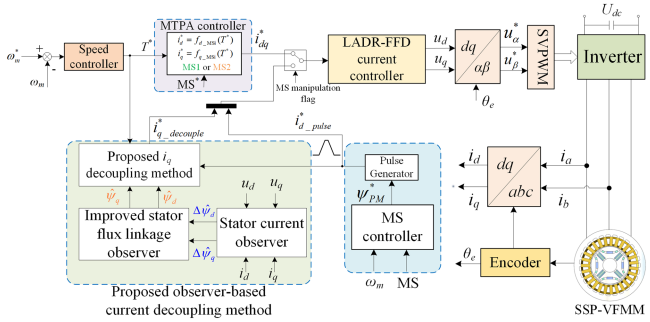

Fig. 9. Schematic diagram of the VFMM speed regulation system.

should be changed from positive to negative to maintain positive electromagnetic torque according to (20), so that large speed fluctuation can be avoided. However, when decoupling the i_q command directly using (20), the calculated i_q will change from positive infinity to negative infinity when ψ_{act} is close to 0. Therefore, a piecewise function is utilized to solve this problem. A threshold value $\psi_{\text{act\_th}}$ is preset and when $\psi_{\text{act}} < \psi_{\text{act\_th}}$, i_q will be set as 0 to avoid the divergence. The decoupled i_q reference can be calculated as

$$i^*_{q\_\text{decouple}} = \begin{cases} 0, & |\hat{\psi}_{\text{act}}| < \psi_{\text{act\_th}} \\ \dfrac{T^*}{1.5p\hat{\psi}_{\text{act}}}, & |\hat{\psi}_{\text{act}}| \geq \psi_{\text{act\_th}}. \end{cases} \tag{23}$$

The schematic diagram of the proposed current decoupling method is shown in Fig. 8. The estimation accuracy of the parameters used in Fig. 8 can be guaranteed through the rigorous derivation in Section IV-A, and will be fully validated through both the simulation and experimental results in the following parts.

C. VFMM Speed Regulation System

Fig. 9 shows the schematic diagram of the speed regulation system for VFMMs. During the normal operation, the dq-axis current commands are generated through a maximum torque per ampere (MTPA) controller. The functions between the dq-axis currents and T^* at MS_i under the MTPA control, i.e., f_{d_MSi} and f_{q_MSi}, are commonly measured in advance and embedded in the controller for real-time invocation, as shown in Fig. 10. During MS manipulation, the MS controller will generate the required i_d current pulse, $i^*_{d\_\text{pulse}}$, to magnetize or demagnetize the machine to the desired MS. In this process, the decoupled i_q command, $i^*_{q\_\text{decouple}}$, is calculated through the proposed

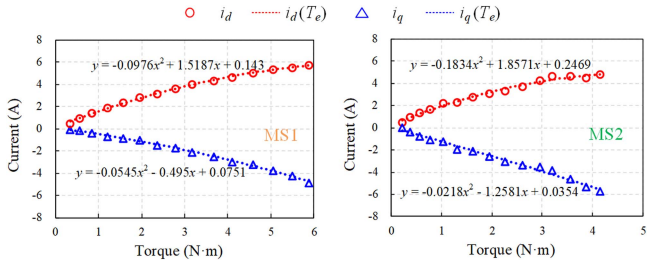

Fig. 10. Experimental MTPA trajectories (i_{dq}- T_e) under MS1 and MS2.

TABLE I
MAIN PARAMETERS OF THE SIMULATION MODEL

Controller/Method	Parameters
PI speed controller	K_p= 0.6, K_i = 10
LADR-FFD current controller	K_{pd} = 20, K_{pq} = 50, bandwidth ω_0=200
Conventional PI regulator	K_p = 20, K_i =100
Proposed STSM regulator	L =100, K_1=15, K_2=110
Proposed current decoupling	i_{qth} = 1 A, ψ_{act_th} = 0.04Wb

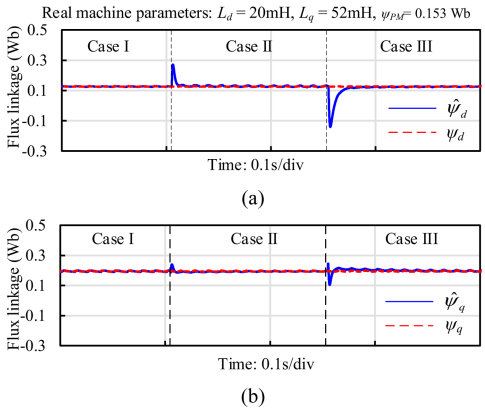

Fig. 11. Simulated waveforms of estimated dq-axis stator flux linkages under 2 N·m load condition, at MS1, with mismatched machine parameters (case I: L_{dN} = 10 mH, L_{qN} = 50 mH, ψ_{PMN} = 0.15 Wb; Case II: L_{dN} = 20 mH, L_{qN} = 30 mH, ψ_{PMN} = 0.2 Wb; Case III: L_{dN} = 30 mH, L_{qN} = 90 mH, ψ_{PMN} = 0.1 Wb).

method to reduce the torque pulsation and speed fluctuation. Then, a linear-active-disturbance-rejection feedforward decoupling (LADR-FFD) current controller [18] is utilized to improve the current tracking performance.

V. SIMULATION VALIDATION

Based on the schematic diagram in Fig. 9, a simulation model of the studied SSP-VFMM is established by using the MATLAB/Simulink to validate the effectiveness of proposed method. A PI speed controller and an LADR-FFD current controller with constant parameters are used in all the simulations and experiments to ensure the fairness of the comparison. The main parameters of the simulation model are listed in the Table I. First, the simulated waveforms of the estimated dq-axis stator flux linkages by using the proposed observer are given in Fig. 11,

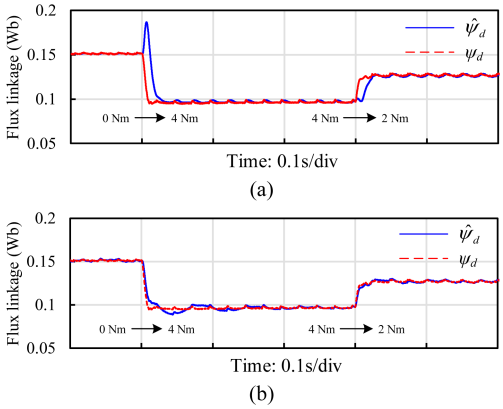

Fig. 12. Simulated waveforms of estimated d-axis stator flux linkage under load change conditions, at MS1. (a) Conventional flux observer. (b) Proposed flux observer.

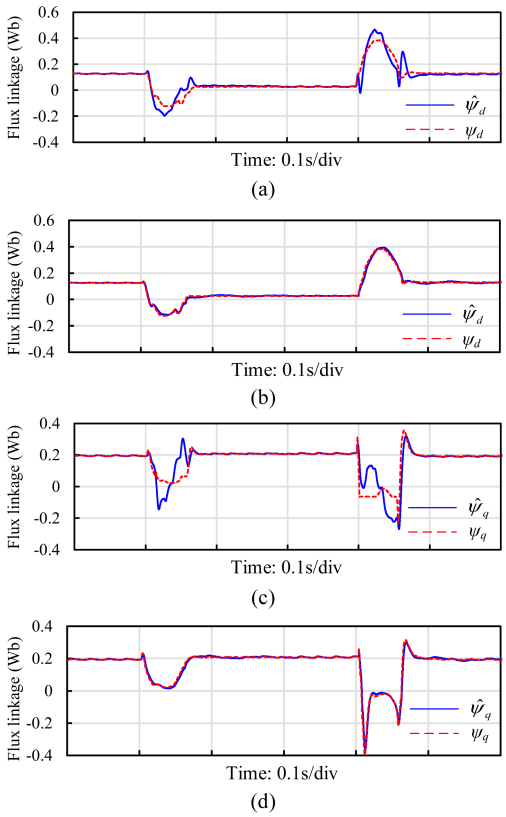

Fig. 13. Simulated waveforms of estimated dq-axis stator flux linkages during two MS manipulations under 2 N·m load. (a) and (c) Conventional flux observer. (b) and (d) Proposed flux observer.

in which the mismatched machine parameters (Cases I, II, and III) are used. In Case I, $L_{dN} = 10$ mH, $L_{qN} = 50$ mH, and $\psi_{\mathrm{PMN}} = 0.15$ Wb, corresponding to the scenario of L_d mismatch. In Case II, $L_{dN} = 20$ mH, $L_{qN} = 30$ mH, and $\psi_{\mathrm{PMN}} = 0.2$ Wb, corresponding to the scenario of L_q and ψ_{PM} mismatches. In Case III, $L_{dN} = 30$ mH, $L_{qN} = 90$ mH, and $\psi_{\mathrm{PMN}} = 0.1$ Wb, corresponding to the scenario of L_d, L_q, and ψ_{PM} mismatches. When using the mismatched values of L_d, L_q, and ψ_{PM} in the three cases, ψ_d and ψ_q can still be accurately estimated, validating that the proposed flux observer is insensitive to the variations of inductances and PM flux linkage.

Then, the simulated estimation performance of d-axis stator flux linkages using different flux observers under load change conditions, at MS1, is shown in Fig. 12. The load changes from 0 to 4 N·m at 0.1 s, and from 4 to 2 N·m at 0.4 s. It can be seen that when using the proposed flux observer considering the dynamic changes of machine parameters, the estimated $\hat{\psi}_d$ can track the real value more accurately than using the conventional observer.

Fig. 13 presents the simulated waveforms of the estimated dq-axis stator flux linkages during two MS manipulations under 2 N·m load, when using conventional and proposed flux observers, respectively. It can be seen that the proposed flux observer can accurately estimate the drastically changed flux linkages when injecting –25 and +30 A i_d pulses, which is much better than the conventional flux observer.

Fig. 14 shows the simulated waveforms of speed and torque during the two MS manipulations when using Methods I, II, and III, respectively. In Methods I and II, the same conventional flux observer is used, and the only difference is that the proposed current decoupling method is used in Method II, whilst the conventional one is used in Method I. It can be seen that the speed fluctuations and torque pulsations during the two MS manipulations are greatly reduced when using Method II compared with those when using Method I, validating the effectiveness of the proposed current decoupling method. In Methods II and III, the proposed current decoupling method is used, and the difference is that the proposed flux observer is used in Method III, while the conventional one is used in Method II. It can be seen that the speed fluctuations and torque pulsations are further reduced when using Method III, validating the effectiveness of the proposed flux observer.

Fig. 15 shows the simulated speed waveforms during two MS manipulations when using different methods under load change conditions. For Method I, the speed fluctuations are very large at the three load conditions due to the drawbacks of the conventional decoupling method, as analyzed in Section III-D. When using both Method II and Method III, the caused speed fluctuations are consequently increased with the load. The speed fluctuations when using Method III are always lower those using Method II under the same load condition, validating the effectiveness the proposed flux observer.

Fig. 16 shows the simulated speed waveforms during the two MS manipulations when using different methods under different reference speed conditions. It can be seen that the magnitude of the speed fluctuations almost keeps unchanged under three different reference speeds when using the same method. The speed fluctuations when using Method III are always lower than those when using Method II, and much lower than those when using Method I, validating the effectiveness the proposed current decoupling method and flux observer.

In summary, the simulation results demonstrate that the proposed flux observer is insensitive to the variations of inductances and PM flux linkage, and exhibits good estimation performance under both load change and MS manipulation conditions.

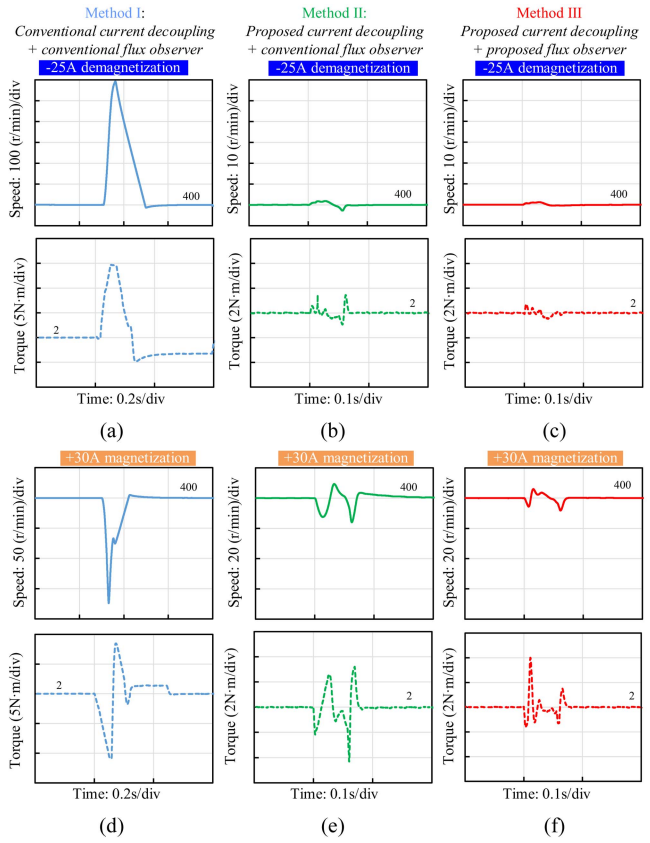

Fig. 14. Simulated speed and torque waveforms during two MS manipulations (–25 A demagnetization and +30 A magnetization) under 2 N·m load and 400 r/min speed using three different methods. (a)–(c) Methods I, II, and III, respectively, during −25 A demagnetization. (d)–(f) Methods I, II, and III, respectively, during +30 A magnetization.

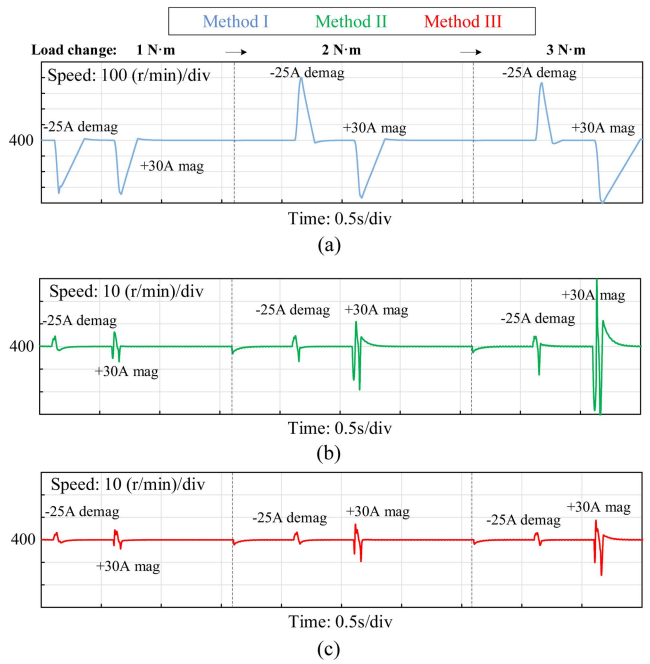

Fig. 15. Simulated speed waveforms during two MS manipulations (–25 A demagnetization and +30 A magnetization) under load change conditions (1, 2, and 3 N·m loads) using three different methods. (a) Method I. (b) Method II. (c) Method III.

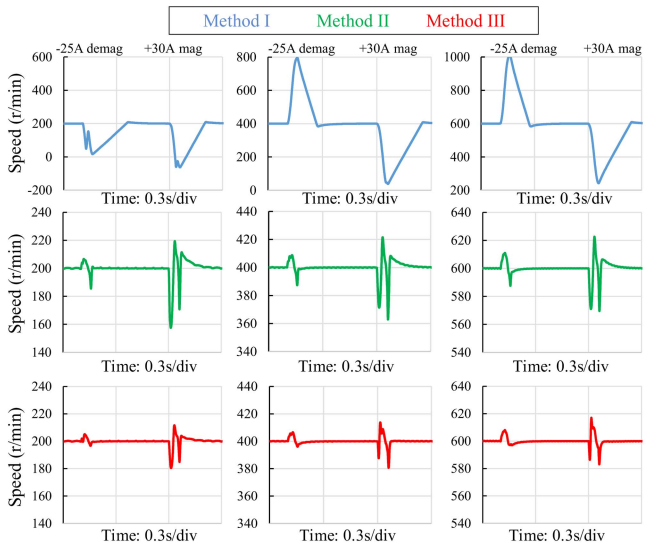

Fig. 16. Simulated speed waveforms during two MS manipulations (–25 A demagnetization and +30 A magnetization) under different reference speeds conditions (200, 400, and 600 r/min speeds) using three different methods.

TABLE II
MAIN PARAMETERS OF SSP-VFMM PROTOTYPE [9]

Symbol	Quantity	Value
U_{dc}	DC bus voltage	120 V
P_N	Rated power	500 W
n_N	Rated speed	800 rpm
p	Pole pairs	2
I_N	Rated current	7.5 A
ψ_{PM1}	PM flux linkage at MS1	0.153 Wb
ψ_{PM2}	PM flux linkage at MS2	0.076 Wb
R	Phase resistance	1.8 Ω
L_{d0}	No-load d-axis inductance	24 mH
L_{q0}	No-load q-axis inductance	54.5 mH
i_{qth}	Threshold of i_q	1 A
ψ_{act_th}	Threshold of ψ_{act}	0.04 Wb

Moreover, the speed fluctuations during the MS manipulations are greatly reduced by using the proposed observer-based current decoupling method (Method III) under different speed and load conditions.

VI. EXPERIMENTAL VALIDATION

The experimental setup for validating the proposed method is shown in Fig. 17. A servo machine is connected with the studied SSP-VFMM through a high-precision torque sensor. The servomachine cannot only drag the tested machine to measure the back electromotive forces, but also serve as a load, which can be flexibly changed through the MEA testing system. An STM32F407VET6 processor is used to implement the control methods. The FreeMASTER debugging tool is utilized to conveniently control the machine in real time and export the required variables into data for postprocessing. The main parameters of the prototype are tabulated in Table II. Besides, the experimental torque-speed curves of the machine at MS1 and MS2 are shown

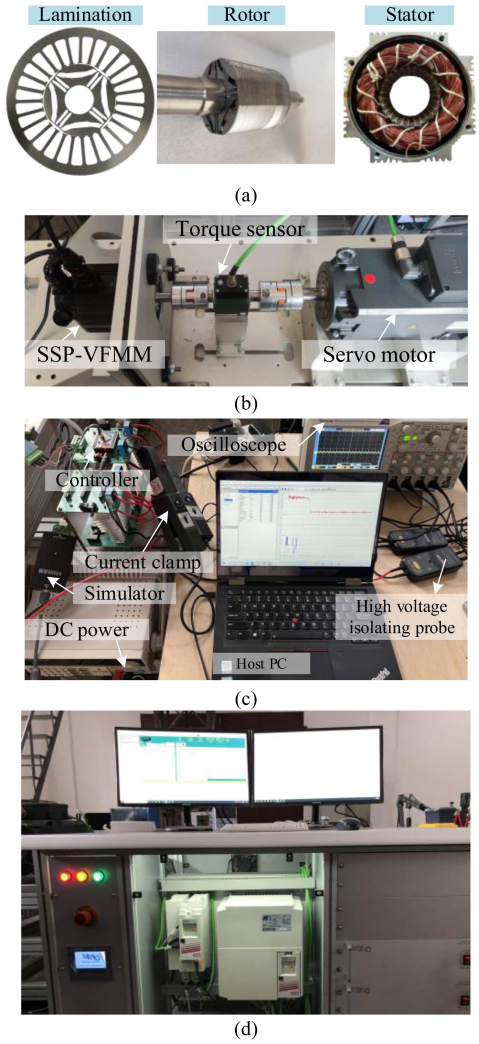

Fig. 17. Experimental setup. (a) SSP-VFMM prototype. (b) Test rig. (c) Control board. (d) MEA testing system.

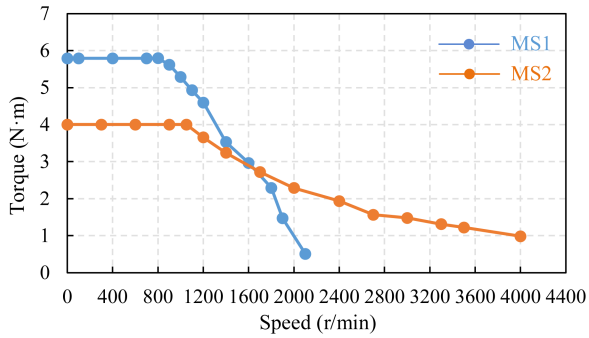

Fig. 18. Experimental torque–speed curves at MS1 and MS2, respectively.

in Fig. 18, in which the speed range can be extended over five times of the rated speed. The rated speed is defined as the corner speed of the torque–speed curve at MS1. It should be noted that the speed range of the machine can be further expanded by adopting a lower MS. It also should be noted that more MSs can be used if necessary, and the accurate MS control and the switch between the MSs can be easily obtained when the

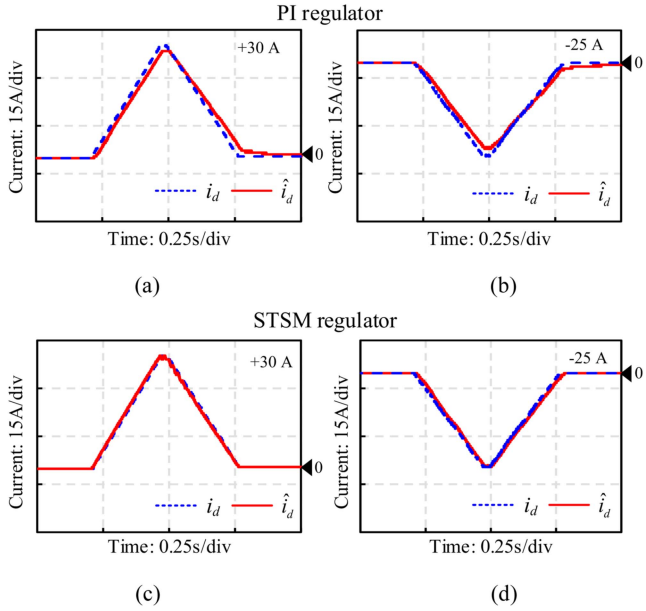

Fig. 19. Experimental d-axis current estimation performance using the stator current observers with different regulators during two MS manipulations, under 400 r/min, 0 N·m conditions. (a)–(b) Using PI regulator. (c)–(d) Using STSM regulator.

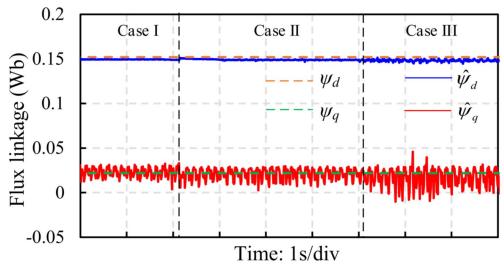

Fig. 20. Experimental waveforms of the real and estimated dq-axis stator flux linkages under 0 N·m load, at MS1, with mismatched machine parameters (Case I: $L_{dN} = 25$ mH, $L_{qN} = 55$ mH, $\psi_{\mathrm{PMN}} = 0.15$ Wb; Case II: $L_{dN} = 10$ mH, $L_{qN} = 10$ mH, $\psi_{\mathrm{PMN}} = 0.05$ Wb; Case III: $L_{dN} = 70$ mH, $L_{qN} = 70$ mH, $\psi_{\mathrm{PMN}} = 0.2$ Wb).

required i_d pulses are applied in sequence. Besides, the multiple MSs will not affect the effectiveness of the proposed method in this article, since it is independent on the current MS, as derived in Section IV.

Fig. 19 shows the experimental waveforms of the real and estimated d-axis currents during two MS manipulations using the conventional (PI regulator) and the proposed (with STSM regulator) stator current observers, respectively. It can be seen that when using the proposed current observer, the estimated currents can better track the real currents, indicating that the voltage disturbances can be more accurately estimated.

Fig. 20 shows the experimental waveforms of the estimated dq-axis stator flux linkages at MS1 with mismatched machine parameters. The calculated real dq-axis flux linkages using the tested machine parameters under 0 N·m load condition are also shown in Fig. 20 with dashed lines. It can be seen that the estimated flux linkages are close to the real values and keep unchanged even using the mismatched parameters in Cases II

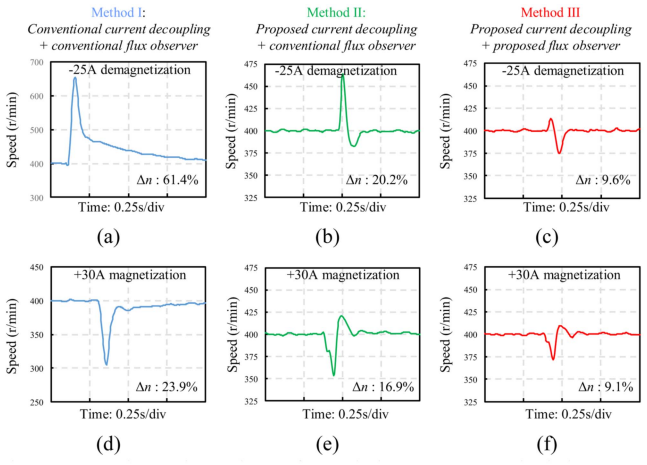

Fig. 21. Experimental speed waveforms during two MS manipulations (–25 A demagnetization and +30 A magnetization) under 1 N·m load and 400 r/min speed using three different methods. (a)–(c) Methods I, II, and III, respectively, during −25 A demagnetization. (d)–(f) Methods I, II, and III, respectively, during +30 A magnetization.

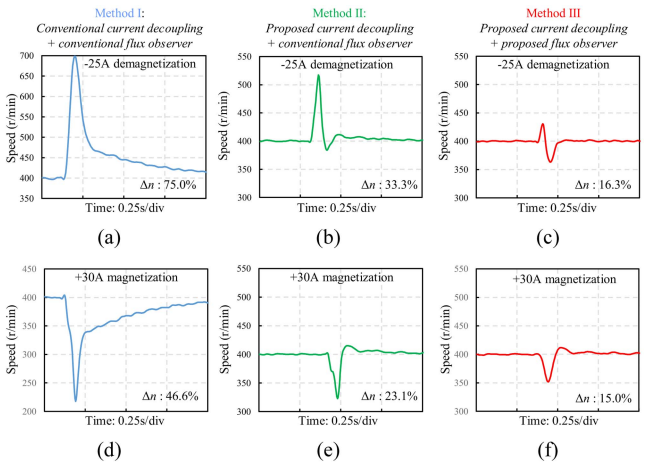

Fig. 22. Experimental speed waveforms during two MS manipulations (–25 A demagnetization and +30 A magnetization) under 2.5 N·m load and 400 r/min speed using three different methods. (a)–(c) Methods I, II, and III, respectively, during −25 A demagnetization. (d)–(f) Methods I, II, and III, respectively, during +30 A magnetization.

TABLE III
PERFORMANCE COMPARISON UNDER DIFFERENT LOAD CONDITIONS

	1 N·m load		2.5 N·m load	
	–25A demag	+30 A mag	-25 A demag	+30 A mag
Method I	61.4%	23.9%	75.0%	46.0%
Method II	20.2%	16.9%	33.3%	23.1%
Method III	9.6%	9.1%	16.3%	15.0%

and III, indicating that the proposed flux observer is insensitive to the variations of *dq*-axis inductances and PM flux linkage.

Figs. 21 and 22 present the experimental speed waveforms during the two MS manipulations when using Methods I, II, and III, under 1 and 2.5 N·m loads, respectively, and the speed fluctuations are listed in Table III for intuitive comparison. In Method I using conventional current decoupling method, the speed fluctuation ratios during –25 and +30 A MS manipulations are very large, 61.4% and 23.9% in Fig. 21, respectively, which are resulted from the fact that i_q is not completely decoupled and the divergence of i_q is not considered. Compared with Method I, Method II can reduce the speed fluctuations to 20.2% and 16.9% during the two MS manipulations, respectively, validating the effectiveness of the proposed current decoupling method. Then, the speed fluctuation ratios under Method III can be further reduced to 9.6% and 9.1% during the two MS manipulations compared with those under Method II, validating the effectiveness of the proposed flux observer. The same conclusion can be drawn through analyzing the experimental results under 2.5 N·m load conditions. It should be noted that though the computation load of Method III is slightly increased compared with Methods I and II, including several multiplication and division operations etc., it can be completed in a very short time by the embedded microprocessor.

This article aims to achieve low torque pulsations and speed fluctuations during MS manipulations under sufficient voltage condition, so that the reference speed is set as 400 r/min in the experiments, which is relatively low. As for conducting the MS manipulations at higher speed conditions, the *q*-axis current should be controlled to obtain a sufficient voltage margin for applying *d*-axis pulses. Several methods have been proposed in [20], [21], [22] to achieve the high-speed capability of MS manipulations, and more details can be found in them.

To more intuitively compare the conventional and proposed flux observers, the experimental waveforms of *dq*-axis currents and flux linkages during the two MS manipulations are shown in Figs. 23 and 24. In Fig. 23, the estimated $\hat{\psi}_d$ and $\hat{\psi}_q$ are distorted during MS manipulations when using conventional flux observer. In contrast, in Fig. 24, the waveforms of the estimated $\hat{\psi}_d$ and $\hat{\psi}_q$ are much smoother and more similar to the current waveforms using the proposed flux observer, indicating that it has better estimation performance. With the

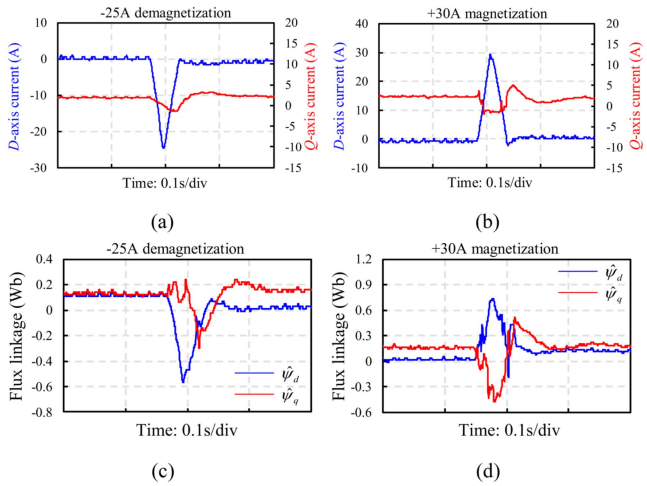

Fig. 23. Experimental waveforms of *dq*-axis currents and estimated stator flux linkages during the two MS manipulations under 1 N·m load using method II. (a) and (b) *Dq*-axis currents. (c) and (d) Estimated *dq*-axis stator flux linkages.

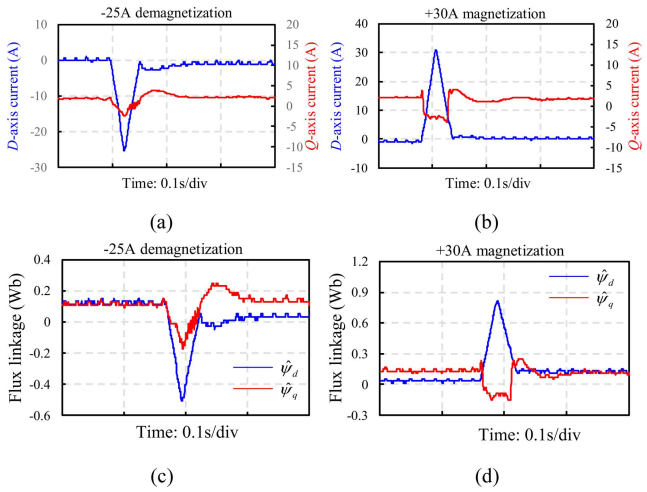

Fig. 24. Experimental waveforms of *dq*-axis currents and estimated stator flux linkages during the two MS manipulations under 1 N·m load using method III. (a) and (b) *Dq*-axis currents. (c) and (d) Estimated *dq*-axis stator flux linkages.

more accurately estimated flux linkages, the decoupled i_q can help better reduce the speed fluctuations, thus the Method III has better performance than Method II.

In practical terms, the speed fluctuations during the MS manipulations can be greatly reduced when using the proposed strategy, significantly improving the speed control performance and the stability of the drive system. This can promote the applications of VFMM in wide speed operations, such as electrical vehicles and washing machines.

VII. Conclusion

The main conclusions and contributions of this article to the control of VFMM are summarized as follows.

1) The proposed improved stator current observer with the STSM regulator can greatly improve the estimation accuracy of current and voltage disturbance at the same time.
2) The proposed improved VDD stator flux linkage observer can accurately estimate the *dq*-axis stator flux linkages during MS manipulations since the dynamic changes of machine parameters are considered.
3) The proposed new observer-based current decoupling method can effectively address the divergence of i_q by using the piecewise function when $\psi_{\rm act}$ is close to 0 and greatly mitigate speed fluctuations during MS manipulations.

The simulation and experimental results on an SSP-VFMM prototype have validated the effectiveness of the proposed current observer, flux observer, and current decoupling method, and the speed fluctuations during MS manipulations can be greatly reduced by using the proposed observer-based current decoupling method.

In the future, the detailed comparison should be made between the flux observer-based and high-performance speed controller-based methods to identify their advantages and disadvantages in speed fluctuation mitigation for VFMMs. Besides, the researchers should investigate on improving the high-speed capability of MS manipulations before reaching the voltage limit of the inverter.

References

[1] T. Jahns, "Getting rare-Earth magnets out of EV traction machines: A review of the many approaches being pursued to minimize or eliminate rare-earth magnets from future EV drivetrains," *IEEE Electrific. Mag.*, vol. 5, no. 1, pp. 6–18, Mar. 2017.
[2] M. Peña, M. Meyer, O. Wallscheid, and J. Böcker, "Model predictive direct self-control for six-step operation of permanent-magnet synchronous machines," *IEEE Trans. Power Electron.*, vol. 38, no. 10, pp. 12416–12429, Oct. 2023.
[3] K. T. Chau, C. C. Chan, and C. Liu, "Overview of permanent-magnet brushless drives for electric and hybrid electric vehicles," *IEEE Trans. Ind. Electron.*, vol. 55, no. 6, pp. 2246–2257, Jun. 2008.
[4] Y. Chen, C. Liu, S. Liu, and Z. Song, "A new cascaded adaptive deadbeat control method for PMSM drive," *IEEE Trans. Ind. Electron.*, vol. 70, no. 4, pp. 3384–3393, Apr. 2023.
[5] S. Liu, C. Liu, H. Zhao, Y. Liu, and Z. Dong, "Improved flux weakening control strategy for five-phase PMSM considering harmonic voltage vectors," *IEEE Trans. Power Electron.*, vol. 37, no. 9, pp. 10967–10980, Sep. 2022.
[6] S. A. Atashin, H. A. Zarchi, and G. A. Markadeh, "Online adaptive current vector adjustment for deep flux-weakening control of IPMSM," *IEEE Trans. Power Electron.*, vol. 38, no. 2, pp. 2339–2350, Feb. 2023.
[7] V. Ostovic, "Memory motors," *IEEE Ind. Appl. Mag.*, vol. 9, no. 1, pp. 52–61, Jan./Feb. 2003.
[8] H. Hua, Z. Q. Zhu, A. Pride, R. Deodhar, and T. Sasaki, "Comparative study on variable flux memory machines with parallel or series hybrid magnets," *IEEE Trans. Ind. Appl.*, vol. 55, no. 2, pp. 1408–1419, Mar./Apr. 2019.
[9] W. Liu, H. Yang, H. Lin, S. Lyu, and Y. Zhong, "A novel variable flux memory machine with separated series-parallel PM structure," *IEEE Trans. Ind. Electron.*, vol. 70, no. 4, pp. 3348–3361, Apr. 2023.
[10] K. Yuuki, K. Sakai, and H. Mochikawa, "Variable-flux motor drive system," U.S. Patent 8 179 068, May 15, 2012.
[11] K. Sakai and K. Yuuki, "Permanent-magnet-type rotating electrical machine and permanent magnet motor drive system," U.S. Patent 8 269 390, Sep. 18, 2012.
[12] K. Yuuki, K. Sakai, and H. Mochikawa, "Variable magnetic flux drive system," U.S. Patent 12/678 929, Sep. 16, 2008.
[13] C.-Y. Yu, T. Fukushige, N. Limsuwan, T. Kato, D. D. Reigosa, and R. D. Lorenz, "Variable-flux machine torque estimation and pulsating torque mitigation during magnetization state manipulation," *IEEE Trans. Ind. Appl.*, vol. 50, no. 5, pp. 3414–3422, Sep./Oct. 2014.
[14] Y. Zhong, H. Lin, J. Wang, Z. Chen, and H. Yang, "Speed fluctuation mitigation control for variable flux memory machine during magnetization state manipulations," *IEEE Trans. Ind. Electron.*, vol. 70, no. 1, pp. 222–232, Jan. 2023.
[15] T. Fukushige, N. Limsuwan, T. Kato, K. Akatsu, and R. D. Lorenz, "Efficiency contours and loss minimization over a driving cycle of a variable flux-intensifying machine," *IEEE Trans. Ind. Appl.*, vol. 51, no. 4, pp. 2984–2989, Jul./Aug. 2015.
[16] A. Athavale, D. J. Erato, and R. D. Lorenz, "Enabling driving cycle loss reduction in variable flux PMSMs via closed-loop magnetization state control," *IEEE Trans. Ind. Appl.*, vol. 54, no. 4, pp. 3350–3359, Jul./Aug. 2018.
[17] J. Chen, J. Li, and R. Qu, "Analysis, modeling, and current trajectory control of magnetization state manipulation in variable-flux permanent magnet machines," *IEEE Trans. Ind. Electron.*, vol. 66, no. 7, pp. 5133–5143, Jul. 2019.
[18] Y. Zhong, H. Lin, Z. Chen, S. Lyu, and H. Yang, "Online-parameter-estimation-based control strategy combining MTPA and flux-weakening for variable flux memory machines," *IEEE Trans. Power Electron.*, vol. 37, no. 4, pp. 4080–4090, Apr. 2022.
[19] K. Yu, Z. Wang, W. Hua, and M. Cheng, "Robust cascaded deadbeat predictive control for dual three-phase variable-flux PMSM considering intrinsic delay in speed loop," *IEEE Trans. Ind. Electron.*, vol. 69, no. 12, pp. 12107–12118, Dec. 2022.
[20] Y. Zhong, H. Lin, J. Wang, W. Liu, and H. Yang, "Q-axis current reverse control of variable flux memory machines with high salient ratio during magnetization process for speed fluctuation reduction," *IEEE Trans. Ind. Electron.*, vol. 71, no. 1, pp. 226–236, Jan. 2024.

[21] B. Gagas, T. Fukushige, T. Kato, and R. D. Lorenz, "Operating within dynamic voltage limits during magnetization state increases in variable flux PM synchronous machines," in *Proc. IEEE Energy Convers. Congr. Expo.*, 2014, pp. 5206–5213.
[22] B. S. Gagas, K. Sasaki, T. Fukushige, A. Athavale, T. Kato, and R. D. Lorenz, "Analysis of magnetizing trajectories for variable flux PM synchronous machines considering voltage, high-speed capability, torque ripple, and time duration," *IEEE Trans. Ind. Appl.*, vol. 52, no. 5, pp. 4029–4038, Sep./Oct. 2016.
[23] W. Xu and R. D. Lorenz, "Reduced parameter sensitivity stator flux linkage observer in deadbeat-direct torque and flux control for IPMSMs," *IEEE Trans. Ind. Appl.*, vol. 50, no. 4, pp. 2626–2636, Jul./Aug. 2014.
[24] I. Boldea, M. C. Paicu, and G.-D. Andreescu, "Active flux concept for motion-sensorless unified AC drives," *IEEE Trans. Power Electron.*, vol. 23, no. 5, pp. 2612–2618, Sep. 2008.
[25] Q. Hou, S. Ding, X. Yu, and K. Mei, "A super-twisting-like fractional controller for SPMSM drive system," *IEEE Trans. Ind. Electron.*, vol. 69, no. 9, pp. 9376–9384, Sep. 2022.
[26] Y.-C. Liu, S. Laghrouche, D. Depernet, A. Djerdir, and M. Cirrincione, "Disturbance-observer-based complementary sliding-mode speed control for PMSM drives: A super-twisting sliding-mode observer-based approach," *IEEE J. Emerg. Sel. Topics Power Electron.*, vol. 9, no. 5, pp. 5416–5428, Oct. 2021.
[27] M. Hinkkanen, T. Tuovinen, L. Harnefors, and J. Luomi, "A combined position and stator-resistance observer for salient PMSM drives: Design and stability analysis," *IEEE Trans. Power Electron.*, vol. 27, no. 2, pp. 601–609, Feb. 2012.

Yuxiang Zhong was born in Jiangsu Province, China, in 1998. He received the B.Eng. degree in electrical engineering from the Nanjing University of Astronautics and Aeronautics, Nanjing, China, in 2019. He is currently working toward the Ph.D. degree in electrical engineering with Southeast University, Nanjing, China.

His research focuses on the control strategies of permanent magnet machines.

Heyun Lin (Senior Member, IEEE) received the B.S., M.S., and Ph.D. degrees in electrical engineering from the Nanjing University of Aeronautics and Astronautics, Nanjing, China, in 1985, 1989, and 1992, respectively.

From 1992 to 1994, he was a Postdoctoral Fellow with Southeast University, Nanjing, China. In 1994, he was an Associate Professor with the School of Electrical Engineering, Southeast University, and has been a Full Professor since 2000. His research interests include the design, analysis, and control of permanent magnet motor, intelligent electrical apparatus, and electromagnetic field numerical analysis. He has authored or coauthored more than 200 technical papers and the holder of 60 patents.

Dr. Lin is a Fellow of IET, a Member of Electrical Motor and Apparatus Committee of Jiangsu Province, and Senior Member of both the China Society of Electrical Engineering and China Electrotechnical Society.

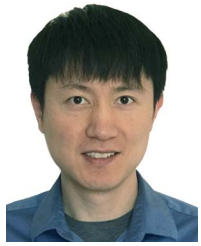

Jiyao Wang (Member, IEEE) received the B.S. degree from Tsinghua University, Beijing, China, and the Ph.D. degree from the University of Wisconsin-Madison, Madison, WI, USA, in 2010 and 2015, respectively, both in electrical engineering.

From 2016 to 2020, he was with Ford Motor Company, Dearborn, MI, USA, where he was part of the Product Development team for the electric motor control and drive system of Ford and Lincoln brand production level electric vehicles including F150 Hybrid, Aviator Hybrid, and Mustang Mach-E. In 2021, he was with the Department of Electrical Engineering, Southeast University, Nanjing, China. His research interests include the designs and controls for the integration of electric machine drive system.

Wei Liu received the B.Eng. degree from the Shandong University of Technology, Zibo, China, in 2015, and the M.Sc. degree from the North University of China, Taiyuan, China, in 2018, both in mechanical engineering, and the Ph.D. degree in electrical engineering from the Southeast University, Nanjing, China, in 2022.

Since 2022, he has been with the Ningbo Institute of Materials Technology and Engineering, Chinese Academy of Sciences, Ningbo, China. His research focuses on the design, analysis, and optimization of electrical machine especially variable flux memory machine.

Hui Yang (Senior Member, IEEE) received the B.Eng. degree from the Dalian University of Technology, Dalian, China, in 2011, and the Ph.D. degree from Southeast University, Nanjing, China, in 2016, both in electrical engineering.

From 2014 to 2015, he was supported by the China Scholarship Council through a one-year joint Ph.D. studentship with the University of Sheffield, Sheffield, U.K. Since 2016, he has been with Southeast University, where he has been an Associate Professor with the School of Electrical Engineering. From 2019 to 2020, he was a Postdoctoral Fellow with the School of Electrical Engineering, The Hong Kong Polytechnic University, Hong Kong. He has authored or coauthored more than 80 IEEE Transactions papers, and was a peer Reviewer of more than ten IEEE journals. His research interests include novel permanent-magnet machines and drives with particular reference to variable-flux machines for electric vehicles and renewable energy applications.

Dr. Yang was a recipient of Best Paper Awards in ICEMS 2014, EVER 2015 and ICEMS 2019, EVS 34, and the holder of 40 patents. He is a TPC-Track Chair of IEMDC 2021, and Organizing Committee Chair of CIEEC 2022. He is invited as a tutorial speaker of PESA 2020 and IEMDC 2021. He is an Associate Editor for IEEE TRANSACTIONS ON INDUSTRIAL ELECTRONICS, IEEE TRANSACTIONS ON ENERGY CONVERSION, and Editor for *World Electric Vehicle Journal*.

Xiping Liu received the B.S. degree in electrical engineering from Hohai University, Nanjing, China, in 1999, the M.S. degree in electrical engineering from the Jiangxi University of Science and Technology, Ganzhou, China, in 2004, and the Ph.D. degree in electrical engineering from Southeast University, Nanjing, China, in 2009.

He is currently a Professor with the Department of Electrical Engineering and Automation, Jiangxi University of Science and Technology. His research interests include the analysis and design of permanent magnet synchronous machine, and wind power technology.